Biomicrofluidics ARTICLE scitation.org/journal/bmf

Nanoelectrokinetic bufferchannel-less radial preconcentrator and online extractor by tunable ion depletion layer

Cite as: Biomicrofluidics 13, 034113 (2019); doi: 10.1063/1.5092789
Submitted: 14 February 2019 · Accepted: 14 May 2019 ·
Published Online: 30 May 2019

Sangjun Lee,[1] Sungmin Park,[1] Wonseok Kim,[1,2,3] Suhong Moon,[1,4] Ho-Young Kim,[5,6] Hyomin Lee,[7,a)] and Sung Jae Kim[1,8,9,a)]

AFFILIATIONS

[1]Department of Electrical and Computer Engineering, Seoul National University, Seoul 08826, South Korea
[2]Department of Bioengineering, University of California, Berkeley, Berkeley, California 94720, USA
[3]Berkeley Sensor and Actuator Center, University of California, Berkeley, Berkeley, California 94720, USA
[4]Department of Electrical Engineering and Computer Sciences, University of California, Berkeley, Berkeley, California 94720, USA
[5]Department of Mechanical and Aerospace Engineering, Seoul National University, Seoul 08826, South Korea
[6]Institute of Advanced Machines and Design, Seoul National University, Seoul 08826, South Korea
[7]Department of Chemical and Biological Engineering, Jeju National University, Jeju 63243, South Korea
[8]Inter-University Semiconductor Research Center, Seoul National University, Seoul 08826, South Korea
[9]Nano Systems Institute, Seoul National University, Seoul 08826, South Korea

[a)]**Authors to whom correspondence should be addressed:** fluid@jejunu.ac.kr and gates@snu.ac.kr

ABSTRACT

Among various preconcentration strategies using nanofluidic platforms, a nanoscale electrokinetic phenomenon called ion concentration polarization (ICP) has been extensively utilized due to several advantages such as high preconcentration factor and no need of complex buffer exchange process. However, conventional ICP preconcentrator had difficulties in the recovery of preconcentrated sample and complicated buffer channels. To overcome these, bufferchannel-less radial micro/nanofluidic preconcentrator was developed in this work. Radially arranged microchannel can maximize the micro/nano membrane interface so that the samples were preconcentrated from each microchannel. All of preconcentrated plugs moved toward the center pipette tip and can be easily collected by just pulling out the tip installed at the center reservoir. For a simple and cost-effective fabrication, a commercial printer was used to print the nanoporous membrane as "Nafion-junction device." Various analytes such as polystyrene particle, fluorescent dye, and dsDNA were preconcentrated and extracted with the recovery ratio of 85.5%, 79.0%, and 51.3%, respectively. Furthermore, we used a super inkjet printer to print the silver electrode instead of nanoporous membrane to preconcentrate either type of charged analytes as "printed-electrode device." A Faradaic reaction was used as the main mechanism, and we successfully demonstrated the preconcentration of either negatively or positively charged analytes. The presented bufferchannel-less radial preconcentrator would be utilized as a practical and handy platform for analyzing low-abundant molecules.

INTRODUCTION

Since a preconcentration is an essential step for sensing various low-abundant analytes in bio- and environmental applications,[1–3] a number of mechanical mechanisms such as membrane filtration,[4–6] inertial focusing,[7] acoustophoresis,[8] diffusiophoresis,[9–14] and thermophoresis,[15,16] etc., have been actively investigated. More recently, due to the easiness of electrical operations, electrokinetic techniques such as isotachophoresis,[17,18] field amplified stacking,[19–23] etc., have been competitively reported using micro/nanofluidic platform. Among the technologies, a nanoscale electrokinetics phenomenon called the ion concentration polarization (ICP) mechanism has extensively utilized recently, due to several critical advantages of high preconcentration factor (most of the target analytes from infinite volume of reservoir would be stacked at specific locations

inside a microchannel) and no need of complex buffer exchange processes.[9,24–32] ICP is the electrochemical phenomenon that observed at the interface of the nanoporous membrane and electrolyte solution.[33–41] When a dc voltage bias is applied to the micro/nano hybridized platform which contains electrolyte, the imbalance of ions occurs at both ends of the nanoporous membrane due to the ion selective permeability of the membrane. To balance electroneutrality, an extended space charge (ESC) layer was formed adjacent to the electrical double layer.[42–45] Inside ESC layer, the concentration of cation is higher than that of the anion. This is the typical process of balancing cation and anion in ICP phenomenon rather than water splitting or metal oxidation. In the case of the cation-selective membrane, an ion depletion zone appears at the anodic side of the membrane and an ion enrichment zone appears at the cathodic side of the membrane. Then, the charged molecules in the electrolyte are preconcentrated at the boundary of the ion depletion zone by the force balance between convective drag force and electrophoretic migration in the microchannel.[24,25,46,47] While one can achieve a high preconcentration factor over a 10^6-fold by ICP,[26] it is extremely difficult to recover the preconcentrated plug in the microchannel because the concentration gradient of the preconcentrated plug to the depletion zone is so large that it dissipates momentarily when the voltage bias is turned off for extracting the plug. To overcome this problem, several studies have been conducted to use preconcentrated plug *in situ* such as confining the preconcentrated plug in the oil phase in combination with the droplet generator[48] or immobilizing functionalized beads at the microchannel bottom where the target molecules were preconcentrated for immunoassay.[49–51] However, a simple extraction method without losing the useful preconcentration factor should still be required for downstream analysis.

While two microchannels connected with a nanoporous membrane have been served as a basic platform of the ICP preconcentrator,[24,52] a simple straight microchannel with nanoporous membrane only at the bottom of microchannel have reported to realize the ICP preconcentrator as well.[51,53,54] We had reported this concept for the first time, and this simple device can minimize the unnecessary electrical connections while keeping the similar preconcentration factor so that it would provide more commercializable platform.[51] Eliminating buffer microchannel would greatly save the space so that it provides beneficial freedom for the high degree of multiplexing or radial design. For further enhancement of throughput and easiness of sample recovery, we have invented a radial type microchannel network in 2010 to maximize the microchannel/nano membrane interface, which results in significantly improved throughput.[55] However, this patent was abandoned recently because the bufferchannel-less concept in this patent (Nafion on top of electrode) was hard to be realized, and we have been developing a different bufferchannel-less concept, which is the new bufferchannel-less concept, in this work (straight microchannel with Nafion at the bottom of microchannel). Using this radial concentrator, not only the throughput but also electrokinetic stability[56–62] can be enhanced. Radial configuration confined the preconcentrated sample in each microchannel, and, thus, the effective length scale can be discretized.[35,62–67] In such microconfined environment, undesirable electrokinetic instability can be largely suppressed. Furthermore, the preconcentrated plugs in each radial microchannel receded toward the center so that one can easily extract the whole plugs using a conventional pipette tip at the center. The dynamics of the preconcentrated sample are categorized into two behaviors.[68] If the plug was pinned near the nanojunction, it is called "stacking behavior." If the plug is receded from the nanojunction, which is the case of this work, it is called "propagating behavior." Thus, the plugs of local extremely high concentration in front of each ion depletion zone can be collected at the center, meaning we fully utilized the advantages of ICP preconcentrator. For example, 50 μl of the sample solution can be 5 μl of the preconcentrated sample solution at the center, which is sufficient volume for downstream chip-to-world analysis. This type of ICP device was named as "a bufferchannel-less radial preconcentrator and online extractor." Few other radially structured preconcentrator had already been reported,[69,70] but their basic layout was traditional main microchannel-membrane-buffer microchannel connection so that it could collect the analytes only inside the radially positioned microchannel itself.

In this work, our bufferchannel-less radial preconcentrator can preconcentrate the whole analytes in the inserted pipette tip so that one can achieve both reasonably useful preconcentration factor and easy sample recovery for a direct downstream analysis. Here, we successfully demonstrated that microbead, fluorescent dyes, and dsDNA were preconcentrated and easily extracted. Moreover, since the Nafion based preconcentrator mainly works on negatively charged molecules, silver electrode was printed instead of Nafion for the more general applicable preconcentrator. With printed-electrode preconcentrator, the ion depletion zone was generated using the Faradaic reaction[71,72] as the main mechanism and the negatively charged molecules as well as the positively charged molecules were successfully preconcentrated in this bufferchannel-less radial type device. Therefore, this device is greatly useful in the lab on a chip platform for most of the sample preparation steps in biochemical analysis. Preconcentrating low-abundant molecules at reasonably high amplification factor and easy extraction of the preconcentrated sample would have significant commercial capability.

EXPERIMENTAL METHODS

Device design

In this work, two types of device were demonstrated. The major difference between them was the way they mediated the ion depletion zone. ICP was used to mediate ion depletion zone using nanoporous membrane called as "Nafion-junction device," and Faradiac reaction was employed using printed silver electrode called as "printed-electrode device." Both types have the same operation procedures, and the step-by-step operation procedures were shown in Fig. 1. Buffer solution without analytes was injected into the microchannel by pressure in advance. Then, step (i) was injecting a commercial pipette tip which contained sample solution at the center of each device. Step (ii) is sample loading and preconcentration by applying electric field between the radial electrode and the pipette tip. The polarity of dc electric field was determined by the target analytes, i.e., positive at center and ground at the electrode for negatively charged analytes and vice versa. Then, solvent in the pipette tip flowed out toward the rims by electro-osmotic flow

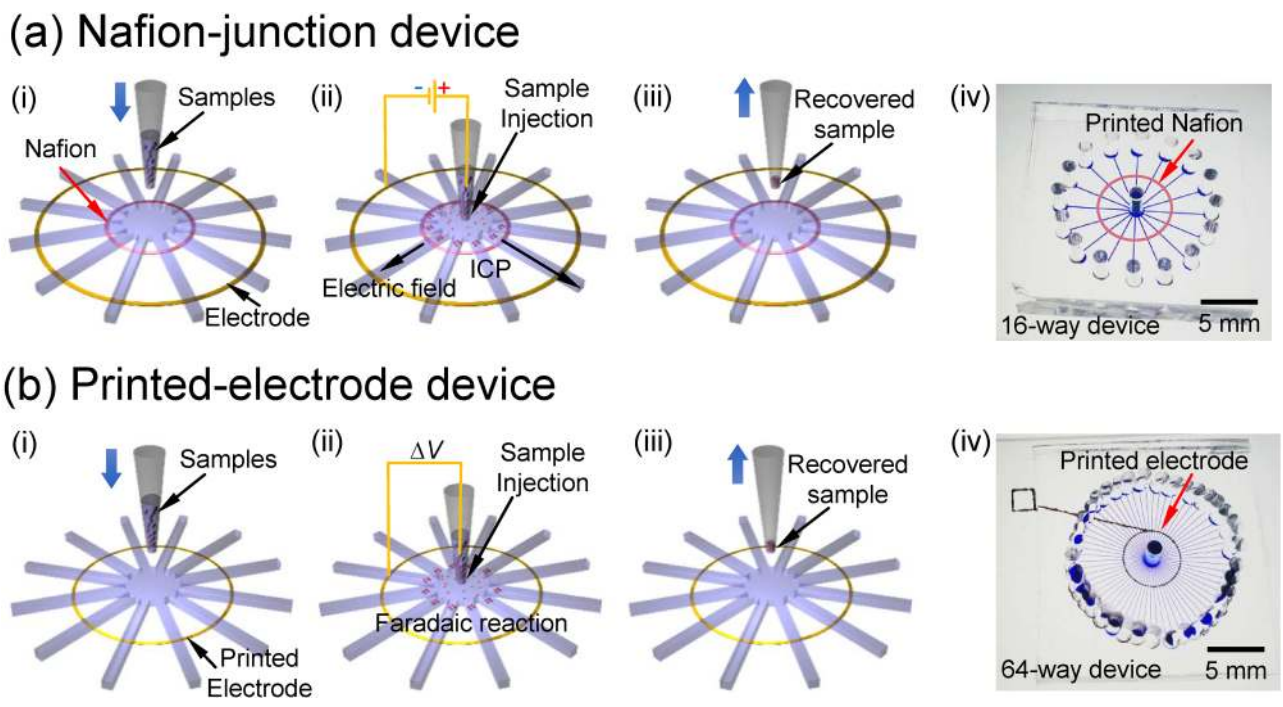

FIG. 1. Schematics of operation procedures and device pictures of (a) Nafion-junction device and (b) printed-electrode device. Both devices had the same operation procedures. (i) Buffer injection and preparation of the sample solution, (ii) sample injection and preconcentration of molecules, (iii) extraction and recovery of preconcentrated molecules, and (iv) photo of fabricated device.

(EOF) and pressure driven flow. Because the depletion zones at each microchannels converged toward the center pipette tip, it prevented the target analytes from flushed outward and all of analytes in the pipette tip were sieved by the depletion boundary, leading high preconcentration factor. Step (iii) is the recovery of the analytes. After removing the solution from all the rims, the pipette tip containing preconcentrated analytes with minimum amount of solvent was pulled out for easy recovery of the analytes. It was expected that the preconcentration and recovery efficiency could be easily increased by changing the number of branch channels of the device or duration time of preconcentration, etc. A fabricated 16 branch channel device with Nafion and 64 branch channel device with printed electrode were also shown in Fig. 1. For the Nafion-junction device and printed-electrode device, each microchannel had the dimension of 100 μm width × 50 μm depth × 7 mm length and the dimension of 50 μm width × 50 μm depth × 7 mm length, respectively. In order to operate ICP at stable conditions, the characteristic length scale should be around O(10) μm as suggested in previous literature studies.[37,63,65] We have tested 75 μm height device, but the results were extremely unstable. This is the consideration for choosing 50 μm height.

Device fabrication

The SU8 microchannel mold was fabricated on the silicon wafer by soft-lithography fabrication method. To replicate the microchannel mold on the polydimethylsiloxane (PDMS, Sylgard 184 Silicon elastomer kit, Dow Corning, USA), a PDMS precursor solution (the mixture of pre-polymer and curing agent at the ratio of 10:1) was poured on the silicon wafer which had microchannel mold and cured in an oven at 75 °C for 4 h. For the Nafion-junction device, Nafion® resin solution (wt. 20%, Sigma-Aldrich, USA) was used as a cation perm-selective membrane. Nafion printing method was used to pattern the atypical shape of nanoporous membrane on the glass using commercial inkjet printer (EPSON, K-100, Japan). Nafion was diluted by DI water at the ratio of 1:7 for matching the viscosity of commercial ink as shown in Table I. On the commercial inkjet printer, diluted Nafion and glass were used instead of commercial ink

TABLE I. The comparison chart of viscosity among the DI water, commercial ink, and diluted Nafion solution.

Material	Viscosity	Nafion vs DI water
DI	1	
Commercial ink	3.89	
Nafion solution	6.15	1:4
Nafion solution	5.32	1:5
Nafion solution	3.26	1:7
Nafion solution	2.49	1:9

and printing paper, respectively, and then, Nafion was simply printed on glass. Finally, printed Nafion was heated on the hot plate at 95 °C to remove the solvent from the Nafion solution, with only solid Nafion solute on the glass remaining.

For the printed-electrode device, silver ink (Silverjet DGP 40LT-15C, Advanced Nano Products, USA) was circularly printed on the glass by a super inkjet printer (SIJ-S030, SIJ Technology, Inc., Japan). Printed silver electrode was heated on the hot plate at 130 °C for 2 h to have 11 $\mu\Omega$ cm of electrical resistivity. Then, PDMS mold with microchannels was bonded with the Nafion patterned (or electrode printed) glass by O_2 plasma treatment (FemtoSience, CUTE-MP, Korea) and cured on the hot plate at 95 °C for 2 h.

Materials

For the Nafion-junction device, the mixture of 1 mM potassium chloride (Sigma-Aldrich, USA) and fluospheres polystyrene [1 μm, blue-green (430/465) particle, Invitrogen, USA], the mixture of 1 mM potassium chloride and Alexa fluorescent dye [Alexa 488, (200 nM), Invitrogen, USA] solution, and 947 bp length of A260 double stranded DNA (Oligonucleotides were customized by Macrogen Inc., Korea) with 0.1× Phosphate-Buffered Saline buffer (Sigma-Aldrich, USA) were used. For the printed-electrode device experiment, the 1 mM Tris–HCl (pH 5.6) solution was prepared by a mixture of tris(hydroxymethyl) aminomethane (Tris base, Sigma-Aldrich, USA) and hydrochloric acid as a buffer, and sulforhodamine B (SRB) (50 nM, Sigma-Aldrich, USA) was used as a negatively charged dye, while rhodamine 6G (50 μM, Sigma-Aldrich, USA) was used as a positively charged dye.

Experimental setup

Viscosity of DI water, commercial ink, and diluted Nafion was measured by a viscometer (SV-10, A&D, Japan). An electrical voltage was applied by source measure unit (Keithley 236, USA) through Ag/AgCl electrode. The behaviors of analytes were traced by an inverted fluorescent microscope (IX-53, Olympus, Japan) and analyzed by ImageJ, CellSense, and spectrophotometer for dsDNA experiment (Qiagen, Germany).

RESULTS AND DISCUSSIONS

As previously stated, experiments were conducted on two types of devices (Nafion-junction device and printed-electrode device). First, Nafion-junction device was demonstrated with preconcentration and extraction of microparticles, fluorescent dye, and dsDNA, and then the printed-electrode device was demonstrated with preconcentration of either positively or negatively charged fluorescent dyes.

Nafion-junction device

Polystyrene microparticle demonstration

To demonstrate the feasibility of bufferchannel-less radial preconcentrator, the preconcentration of 1 μm-size polystyrene microparticle at 1 mM potassium chloride buffer background solution was firstly operated in the 8-way radial preconcentrator, and the fluid motion of microparticles was visualized as shown in Fig. 2(a) (Multimedia view). The image was taken from only 2 channels out of 8 radial channels. After injecting solution into the microchannel, 10 V was applied between center pipette tip and the end of the channel for preconcentration step. With the voltage bias, an ion depletion zone was formed at the anodic side of the Nafion, and microparticles were started to be preconcentrated as shown in Fig. 2(a). Since the strong vortical flow inside the depletion zone induces a weak vortex outside the depletion zone,[37,67,73] the shape of the preconcentrated particles involved both compact plug and vortical cloud at the boundary of the depletion zone. As dc bias was applied continuously at the device, the preconcentrated plug and vortical cloud of microparticles were propagated to the center, while solvent in the center pipette tip was flushed out toward the rim at each branches. After 2 h of operation, most of the microparticles contained in the pipette tip were gathered at the bottom of the pipette tip as shown in Fig. 2(b). In this experiment, 35 μl of the microparticle solution was operated for 2 h to become 3 μl of concentrated solution. The theoretical concentration ratio was calculated by dividing the final volume by the initial volume, which results in about 11.7-fold of preconcentration factor. To calculate the experimental result of concentration ratio after preconcentration, the number density of microparticles at the bottom of the center pipette tip between before and after preconcentration step was compared. Region of interest (ROI) to count the number density was set to be an annular shape as shown in Fig. 2(b). We excluded the center region where the pipette tip was inserted. Before preconcentration step, ~80 particles were counted inside the ROI, while ~800 particles were counted inside the ROI after preconcentration step (particles within the same focal length was only counted). Thus, the measured preconcentration factor after the operation was calculated to be 10-fold. Dividing the experimental concentration ratio by the theoretical concentration ratio, it showed 85.5% of particle recovery ratio as in Fig. 2(c). This result proved that most of the particles were captured by the depletion zone and collected to the center pipette tip. While previously reported preconcentrating techniques can preconcentrate the analytes only in a small volume (few picoliters to nanoliters) of microchannel, the radial preconcentrator in this work has advantages over them since it can collect all the analytes into relatively large volume of pipette tip (few microliters). Although we demonstrated with the 10 μl pipette tip (white tip), we can achieve higher preconcentration ratio if one uses a larger volume of pipette tip (blue tip of 1 ml). However, in this case, the preconcentration time should be longer so that it is necessary to leverage the preconcentration ratio and the operation time according to one's discretion.

Fluorescent dye demonstration

Since we confirmed that most of the particles in the pipette tip were preconcentrated at the bottom of the pipette tip, while the solvent was flushed out, small analytes (200 nM concentration of Alexa 488 fluorescent dye) with 1 mM potassium chloride buffer background solution were used to demonstrate both preconcentration and extraction steps. Figure 3(a) (Multimedia view) showed the preconcentration of fluorescent dye at a 16-way radial device with a voltage of 10 V. At 10 s, fluorescent dyes started to form plugs at each anodic side of Nafion and the preconcentration plugs propagated to the center pipette tip as shown

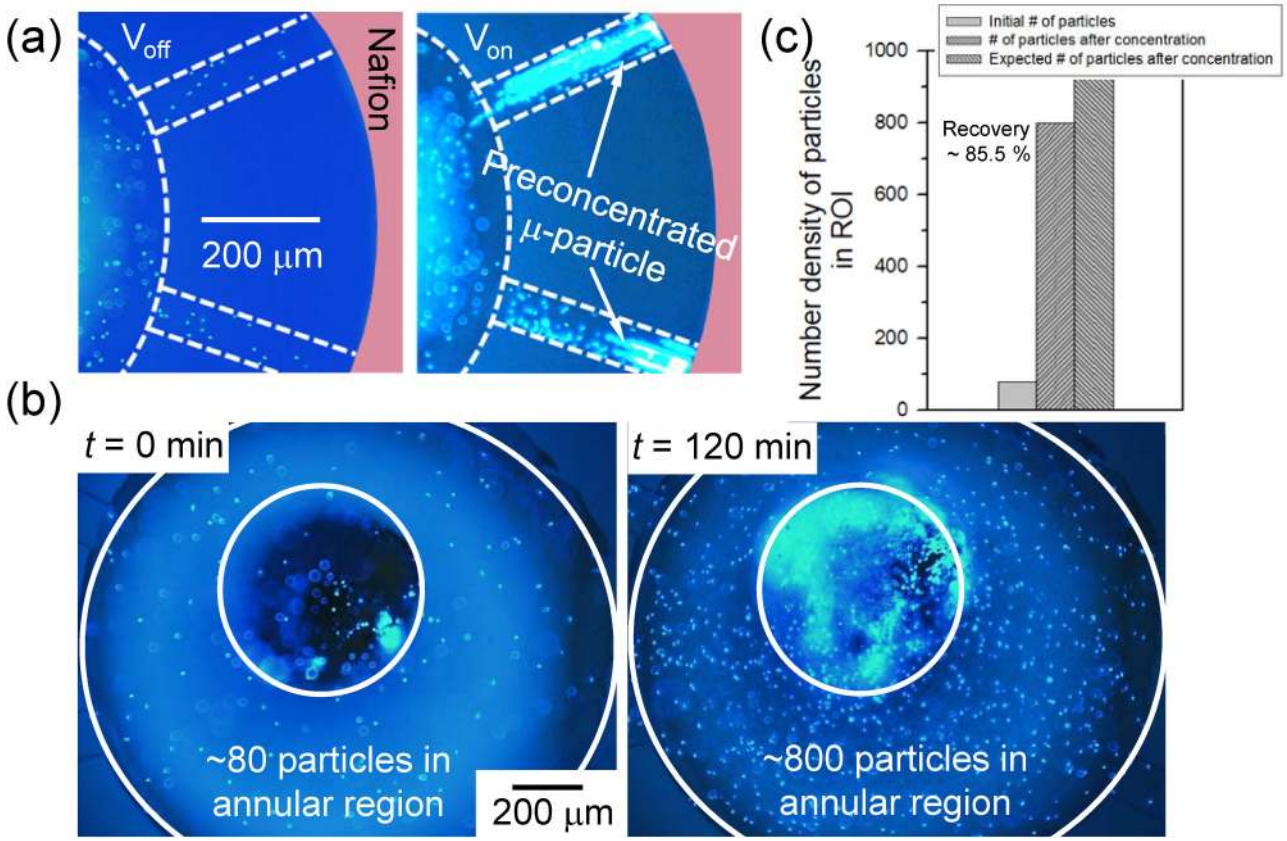

FIG. 2. (a) Microscopic snapshots of microparticle preconcentration, demonstration using Nafion-junction device. When dc bias was applied, particles showed both compact plug with vortical cloud. Multimedia view: https://doi.org/10.1063/1.5092789.1. (b) Microscopic image at the bottom of center pipette tip at $t = 0$ min (before preconcentration, left image) and $t = 120$ min (after preconcentration, right image). Number density of particles at the same focal length in the ROI was compared. (c) Diagram of number density of particles from (b) and number density of particles calculated by the volume ratio before and after preconcentration step.

in the right image of Fig. 3(a) (Multimedia view). In order to quantify the preconcentration efficiency, electro-osmotic velocity ($v_{eof} = \varepsilon_0 \varepsilon_r \zeta |\mathbf{E}|/\mu$, where ε_0 and ε_r are the permittivity of free space and relative permittivity of the sample solution, respectively, μ is the viscosity of the sample solution, ζ is the zeta-potential of microchannel wall, and $|\mathbf{E}|$ is the applied electric field to each microchannel) was calculated for measuring the operation time. Here, the parameters were given as $\varepsilon_0 = 8.854 \times 10^{-12}\,\mathrm{CV^{-1}\,m^{-1}}$, $\varepsilon_r = 80$, $\mu = 0.001\,\mathrm{N\,s\,m^{-2}}$, and $\zeta = \sim -80\,\mathrm{mV}$.[74,75] Since the radial preconcentrator had a parallel connection structure and the length of each channel was fixed at 7 mm, the average electric field across at each branch channel was assumed to be constant at 14 V/m with 10 V constant bias. Then, v_{eof} was calculated to ~80 μm/s on each microchannel. Multiplying the width and height of each microchannel (100 μm and 50 μm, respectively), the volume flow rate induced by electro-osmotic flow (vol_{eof}) was calculated to be ~20 nl/min on each microchannel. Three types of device with 4, 8, and 16 branch channels were prepared to verify device operation time according to electro-osmotic flow and number of channels, and we calculated the time taken for the solution to decrease from 35 μl to 1 μl using the above volume flow rate, giving the operation time as $T_{op} = (V_{initial} - V_{final})/nvol_{eof}$ (where T_{op} the device operation time, $V_{initial}$ and V_{final} the initial and final volume, respectively, and n the number of branch channels). The calculated T_{op}s were ~360 min, ~180 min, and ~90 min for $n = 4$, 8, and 16 branch channels, respectively. Experimental T_{op}s were measured (time taken by the initial volume of 35 μl is reduced to 1 μl) were ~190 min, ~120 min, and ~75 min on average for 4, 8, and 16 branch channels, respectively, as shown in Fig. 3(b). Main reason for the difference between the calculated device operation time and measured device operation time was pressure driven flow. Corresponding flow rates of pressure driven flow are ~20 nl/min, ~10 nl/min, and ~5 nl/min for 4, 8, and 16 branch channels. Since pressure difference was induced by the level difference between center pipette tip and each reservoir at the end of each branch, more branch caused less pressure difference. Thus, the flow rate from pressure driven flow should inversely proportional to the number of branches as we have shown above.

Since 30 μl and 50 μl solution was preconcentrated until $V_{final} = 5\,\mu$l, we aimed to achieve the preconcentration ratio was 6- and

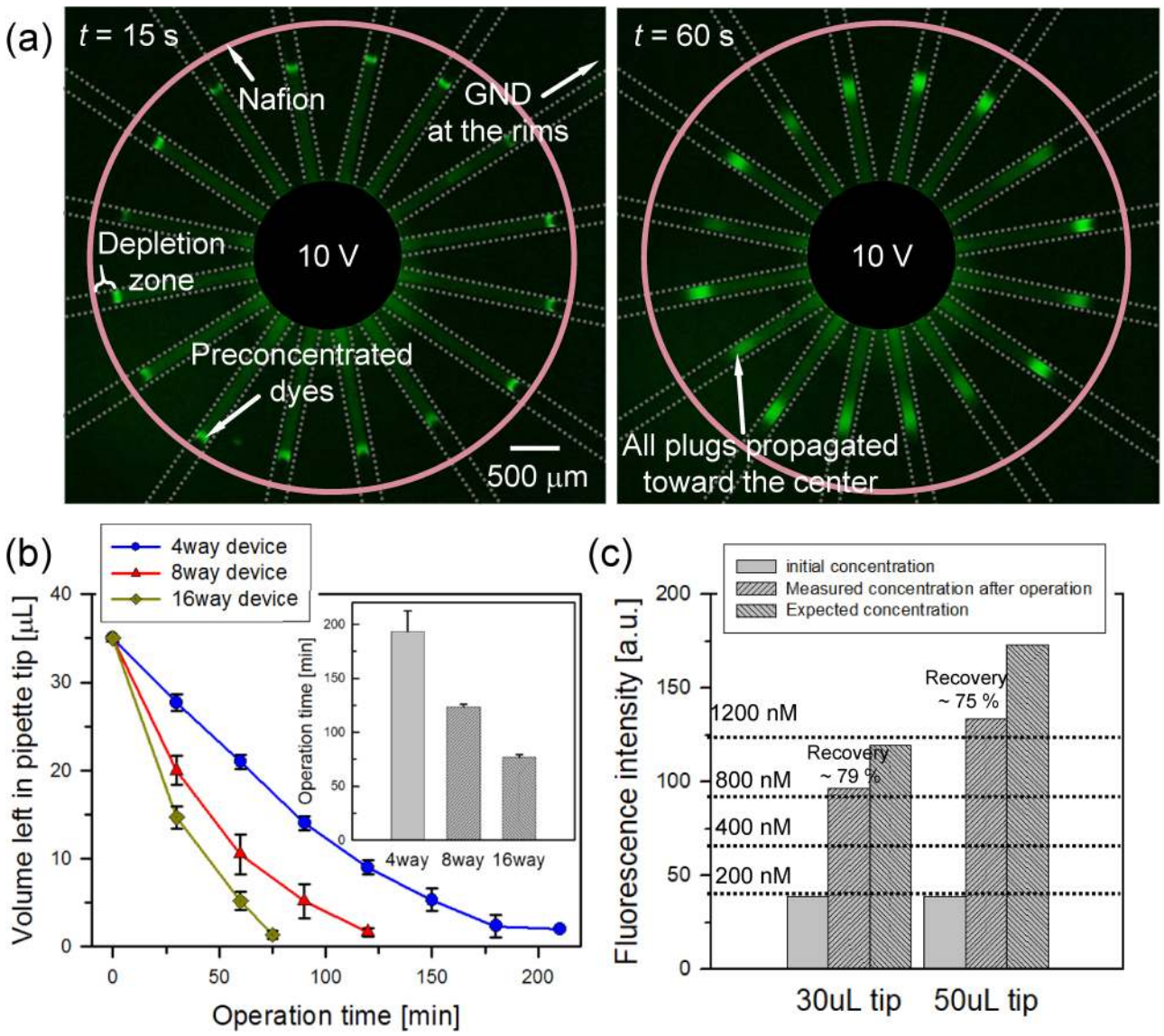

FIG. 3. (a) Microscopic snapshots of fluorescent dye preconcentration demonstration using 16-way Nafion-junction device. Preconcentrated dye plugs formed (left image) and propagated toward the center (right image) with applied dc bias. Multimedia view: https://doi.org/10.1063/1.5092789.2. (b) Graph showed the amount of solution left in the pipette tip as the device operated and the calculated T_{op} for 4-, 8-, and 16-way device. (c) Diagram showed the concentration of $M_{initial}$ and M_{ext} compared to expected concentration by the volume ratio before and after preconcentration step.

10-fold, respectively. In previous ICP works, such as 10^6-fold preconcentrator,[26] the analytes were preconcentrated inside a microchannel, and the factor was measured again inside the microchannel, whereas our radial preconcentrator measured the concentration ratio after extracting the preconcentrated analyte out of the microchannel so that there should be an inevitable dilution occurred in micro-to-world interfacing. With setting the maximum factor as 10^6, one may expect the maximum factor inside microchannel of $100(10^6 \times 100\,\mu\text{m}$ (plug length) $\times\, 100\,\mu\text{m}$ (plug width) $\times\, 50\,\mu\text{m}$ (plug height)$/5\,\mu\text{l})$. However, since our design is "bufferchannel-less" and there should be an inevitable dilution at world-to-chip interfacing, the factor obtained by volume ratio (initial volume/final volume) would provide more accurate estimation than the factor by above simple calculation. While ~10-fold can be considered low, it is expected that one can accomplish a preconcentration ratio higher than 10-folds using a larger pipette tip at the center reservoir.

In order to extract the preconcentrated sample, the solvent at the entire rims was removed first and the remaining preconcentrated

solution at the center was extracted by just pulling out the pipette. The extracted solution was injected into straight microchannel of 15 μm height and 100 μm width, and the intensity of the fluorescent dye was analyzed using ImageJ. Recovery ratio of the dye was calculated as $R = V_{ext}M_{ext}/V_{initial}M_{initial}$, where V_{ext} the extracted solution volume and $M_{initial}$ and M_{ext} the initial and extracted molar concentration of the dye, respectively. The value of R by the experimental data gave ~79%, and ~4.5-fold of preconcentration factor for 30 μl solution and ~75%, and ~7.5-fold of preconcentration factor for 50 μl as shown in Fig. 3(c). We expected the preconcentration ratio (the ratio of the initial sample volume to the recovered sample volume) of 6-fold when we injected 30 μl of the initial sample and recovered 5 μl of the preconcentrated sample. In the case of 50 μl initial volume, the recovered volume was 5 μl so that the expected value was 10-fold. However, experimentally measured preconcentration ratio was 4.5-fold and 7.5-fold. This small discrepancy against the expected preconcentration ratio was due to the natural diffusion before dc bias was applied and the sample loss due to induced advection when the pipette tip was pulled out from the device.

dsDNA demonstration

The preconcentration and extraction of dsDNA were also conducted to verify the possibility of the radial preconcentrator/extractor to BioMEMS applications. The initial concentration of dsDNA

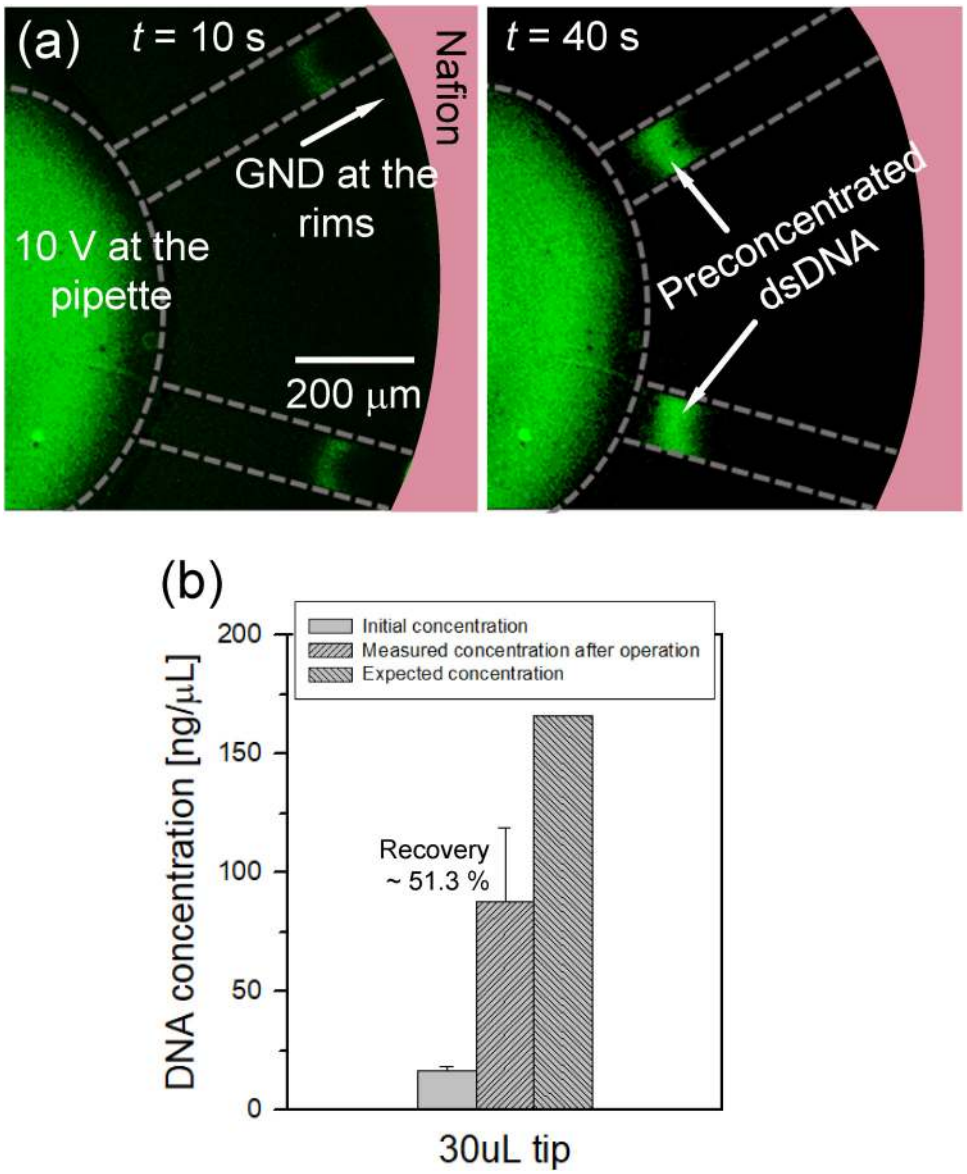

FIG. 4. (a) Microscopic snapshots of dsDNA preconcentration demonstration using Nafion-junction device. Multimedia view: https://doi.org/10.1063/1.5092789.3. (b) Diagram showed the concentration of $M_{initial}$ and M_{ext} compared to expected concentration by the volume ratio before and after preconcentration step.

was ~16.6 ng/μl with 0.1× PBS, and 10 V bias was continuously applied at 8-way radial device. As shown in Fig. 4(a) (Multimedia view), preconcentrated plugs of dsDNA was successfully converged to the center pipette tip, while solvent was flushed out toward the rims. After the preconcentration step, preconcentrated samples were extracted in the same manner as the fluorescent dye experiment, expecting 10-fold of the preconcentration ratio (30 μl sample solution was preconcentrated to 3 μl). The extracted solution was analyzed with the spectrophotometer, and the results are shown in Fig. 4(b). The concentration of DNA extracted from the center pipette tip was measured to be 87.8 ng/μl on average with a standard deviation of 31.2, showing a concentration ratio of ~4.9-fold compared to the initial concentration. Considering $V_{initial}$ and V_{ext}, the expected concentration ratio was 10-fold. The measured preconcentration ratio of dsDNA showed large deviations due to the same reason stated in the previous section. Furthermore, dsDNA has lower zeta potential[76] than that of the fluorescent dye[77] used in this work, leading to high probability of leaking through the ion depletion zone (i.e., lower preconcentration factor). The recovery ratio, R, by the experimental data gave ~51.3% of dsDNA.

With a view of recovering preconcentrated sample for chip-to-world analysis, this bufferchannel-less radial preconcentrator has advantages over previously reported radial preconcentrator.[69] It demonstrated two types of radial preconcentrator: (i) empty chamber type and (ii) finned chamber type. The empty chamber type has a chamber volume of 100 nl ($\pi \times 1.2\ \text{mm}^2 \times 20\ \mu\text{m}$) and a preconcentrated sample volume of 20 nl ($700 \times 700 \times 40\ \mu\text{m}^3$), and the preconcentration factor was measured at 168-fold. Thus, there should be 1/250-fold dilution for chip-to-world analysis, if 20 nl of 168-folded sample was extracted by laboratory apparatus such as pipette. (We assumed that 5 μl is the minimum volume for delivering the sample to another conventional analyzer.) Also, the finned chamber type has a chamber volume of 1.5 μl ($\pi \times 3.5\ \text{mm}^2 \times 40\ \mu\text{m}$) and a preconcentrated sample volume of 10 nl ($400 \times 700 \times 40\ \mu\text{m}^3$), and the preconcentration factor was measured to be 20-fold. Thus, there should be 1/500-fold dilution for chip-to-world analysis, if 10 nl of 20-folded sample was extracted by the laboratory apparatus. Furthermore, both structures can preconcentrate the sample, which was already filled inside the chamber so that the extracted sample volume is always limited by the chamber volume. Therefore, this comparison led that these previously-developed radial preconcentrators are suitable for chip-to-chip analysis, not for chip-to-world analysis. Note that there should be an additional structure to prevent an avoidable dispersion even in the chip-to-chip analysis.

Printed-electrode device

With the Nafion-junction device, the negatively charged molecules (microparticle, fluorescent dye, and dsDNA) were able to be preconcentrated and extracted because the convective drag force and electrophoretic force affected to the negatively charged molecules in the opposite direction. However, since those forces aligned in the same direction in the case of positively charged species such as rare earth elements, heavy metals, and positively charged amino acids (lysine, arginine, histidine, etc.), it was difficult to preconcentrate positively charged molecules on the cation-selective membrane device. To preconcentrate the positively charged molecules in the ICP preconcentration device, an anion-selective membrane was needed to be used as a nanoporous membrane. However, utilization of either cation- or anion-selective membrane hindered the versatility of the device. Consequently, it is highly required to have a tunable preconcentrating device for either positively or negatively charged analyte at one's discretion. In this work, we fabricated the silver electrode patterned radial preconcentrator for switchable Faradaic reaction on the printed electrode for preconcentrating either type of charged molecules.[71,78] The schematics of the preconcentration by Faradaic reactions at the single straight microchannel were shown in Figs. 5(a) and 5(b) (Multimedia view) for negatively- (50 nM of SRB) and positively charged analyte (50 μM of rhodamine 6G), respectively. Due to the nonspecific binding of the cationic dye to negatively charged PDMS surface, one need to use thicker cationic dye than anionic dye (but they have similar fluorescent intensity); see the supplementary material, Note 1, for details about the electrode reaction. The direction and thickness of blue arrows in Fig. 5(a) corresponded to the directions of electro-osmotic flow (EOF) (along with the applied electric field) and the magnitudes of EOF (greater inside the ion depletion zone than outside the zone due to the amplified electrokinetic response only inside the zone[73]), respectively. In the case of negatively charged molecules, the directions of EOF and electrophoresis (EPH) [$\mathbf{F}_{EPH}$ in Fig. 5(a)] are opposite to each other and are preconcentrated on the same principle as the conventional ICP preconcentration. In the case of positively charged molecules, the directions of EOF and EPH are the same. However, since the forces received by the molecules inside the depletion zone are stronger than the forces received outside the depletion zone, preconcentration occurs with similar principle as isotachophoresis.[17] Without pressure driven flow [red arrow in Figs. 5(a) and 5(b)], the sample flows toward the center pipette so that the sample in the pipette gets diluted. To prevent this backward flow, we intentionally applied pressure driven flow in this printed-electrode device. While the sample was filled from the pipette tip to the reservoir at the ends of radial channels in the Nafion-junction device, the sample was filled from the pipette tip, but the filling was stopped in the middle of microchannels in this printed-electrode device. Thus, the printed-electrode device always has a pressure driven flow toward the rim.

Since major carriers at this reaction were hydrogen ion and chloride ion, we used Tris–HCl buffer as the buffer solution to contain sufficient hydrogen and chloride ions, while keeping the buffer solution as weak acid (pH = 5.6). When voltage was applied to the bulk pipette tip and the printed electrode, reduction and oxidations occurred at the cathode and anode, respectively by the electrochemical reaction. Due to the extremely large resistance of the ion depletion zone, the ionic current through the electrode was less than 10 nA so that the generations of gaseous byproducts were largely suppressed, especially after forming the ion depletion zone. Under this situation, the gaseous byproducts from the electrochemical reactions that generated near the bulk pipette tip were dissolved into the bulk solution so that the ion concentration near the bulk pipette tip was maintained. Any bubbles at patterned electrodes were observed in the experimental condition in this work; see the supplementary material, Note 1, for simple calculation of bubble generation vs solubility. Thus, the ion depletion zone near the printed electrode can be utilized as a preconcentration barrier.

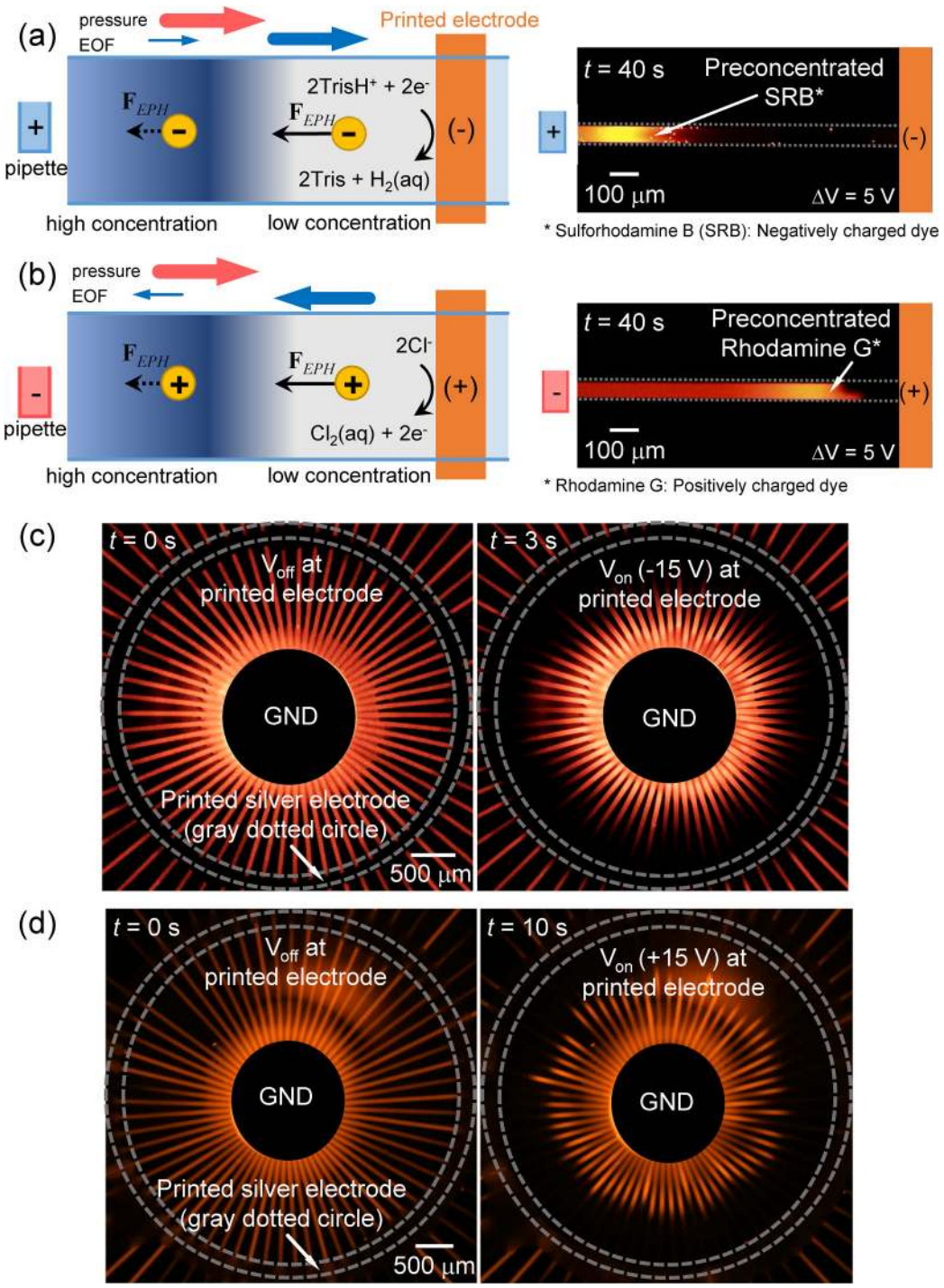

FIG. 5. (a) Schematic diagram for the generation of depletion zone by Faradaic reaction (anode: pipette, cathode: printed electrode) to preconcentrate negatively charged molecules. Microscopic snapshot of SRB demonstration was shown in the right image. (b) Schematic diagram for the generation of depletion zone by Faradaic reaction (anode: printed-electrode, cathode: pipette) to preconcentrate positively charged molecules. Microscopic snapshot of Rhodamine 6G demonstration was shown in the right image. Multimedia view: https://doi.org/10.1063/1.5092789.4. Microscopic snapshots of preconcentration demonstration of (c) SRB and (d) Rhodamine 6G using 64-way printed-electrode device. Multimedia view: https://doi.org/10.1063/1.5092789.5.

When the printed electrode was a cathode, a preconcentrated plug of negatively charged fluorescent dye was formed in the direction to the pipette tip by the electric field gradient caused by the ion depletion zone near the printed electrode [Fig. 5(a)] and vice versa [Fig. 5(b) (Multimedia view)] for positively charged dye. Since the surface charge on the wall of microchannel was negative, positively charged dye received electrical attraction from the channel wall, and the progress of the preconcentration plug was slower than that of the negatively charged dye.

These principles were directly applied to the 64-way radially arranged microchannel. The channels were attached on the printed electrode, and the results were shown in Figs. 5(c) and 5(d) (Multimedia view). The voltage applied at the center pipette tip was fixed as ground for both experiments. To preconcentrate the negatively charged molecules, the printed electrode was used as a cathode and vice versa. The preconcentration plugs of negatively charged dye were formed and started to propagate to the center within only 3 s under 15 V bias [Fig. 5(c); preconcentration factor of 2 within 3 s], while 10 s were needed for the positively charged dye to form plugs and start to propagate to the center [Fig. 5(d); preconcentration factor of 2 within 10 s] under the same dc bias as we expected. Due to gas bubble generation at the patterned electrode and pH variation for a long-term operation exceed an hour, the printed-electrode preconcentrator is better suited for the platform of on/off sample detection using the preconcentrated sample at the center reservoir. However, it is still useful as the preconcentrator and online collector when the target volume is small so that total operation time is less than an hour. Also, patterning the chemically stable metal electrode such as gold or nonpolarizable electrode would be an alternative strategy for longer operations.

CONCLUSIONS

In this work, we proposed a bufferchannel-less micro/nano fluidic device with a simple extraction method while the useful preconcentration factor was maintained for downstream analysis. With the bufferchannel-less design, we minimized the unnecessary electrical connection and employed a radial type microchannel network to maximize the microchannel/nano membrane interface, which results in significantly improved throughput and stability. Most importantly, the preconcentrated samples were easily recovered by just pulling out the center pipette tip. With the Nafion-junction device, ICP was used as the main mechanism and preconcentration of 1 μm-size polystyrene particle was firstly demonstrated to verify the basic operation of the device with the ~85.5% of recovery ratio. The preconcentration and extraction of fluorescent dye and dsDNA were demonstrated, and we could recover ~79.0% and ~51.3% of analytes in the whole pipette tip within analyzable volume, respectively. Operation time of the device was also compared depending on the number of branch channels. With the printed-electrode device, a Faradaic reaction was used as the main preconcentration mechanism. To verify the device operation, preconcentration of either type of charged molecules was demonstrated at the single straight microchannel. Then, these principles were directly applied to the 64-way radially arranged device and preconcentration was successfully demonstrated.

Despite of these advantages, current design was not suitable at high buffer concentrations. We performed additional experiments at 10 mM and 100 mM. The results showed that a constant preconcentration plugs were successfully generated at 10 mM, but serious bubble generation due to electrolysis was observed at 100 mM; see the supplementary material, Note 2. The original bufferchannel-less preconcentrator was demonstrated at 1× PBS condition, but it had only one microchannel.[51] The measured current level in bufferchannel-less device is about 4 times higher than the one in buffered device because the ionic current can flow simultaneously through electrolyte above the membrane and through the membrane. It is more serious in the radial concentrator because the current is linearly proportional to the number of radial branches and the buffer concentration. For example, 10 nA was measured in typical buffered device at 1 mM and 10 V[34] so that ~192 μA should flow in 16 channel bufferchannel-less radial concentrator at 100 mM and 30 V, i.e., 10 nA × 4 (due to bufferchannel-less) × 16 channels × 100 (due to 100 mM) × 3 (due to 30 V). At such huge current, bubble generation on patterned electrode should be non-negligible compared to the microbubble generation at lower current. The ring electrode can be located within an outlet reservoir, allowing the evacuation of generated bubbles. However, as shown in the supplementary material, Fig. S2, the bubble was generated also in the center reservoir as well to disconnect electric field.

This is the clear limitation of this bufferchannel-less radial preconcentrator. Thus, further modifications should require for proper operation at the high concentration such as changing electrode material to suppress electrolysis (for example, a material having higher surface to volume ratio such as carbon felt) or thicker Nafion patterning to minimize leakage current above the membrane and structural modification for removing gas bubble (for example, hydrophobic coating inside the pipette tip and electrode surface leads to easy evacuation of the bubble). However, there are several applications that should work at this low buffer concentration less than 10 mM. For example, environmental monitoring or food monitoring applications usually dealt with tap water from faucet or fresh water from river (or food), etc. whose total ionic concentration is less than 10 mM (10 mM is the upper limit of potable water). A few biological applications also required a dilution at low concentration condition. While drying could be used, it is to concentrate not only the particles but also the electrolyte ions. On the other hand, ICP method concentrates only the particles while maintaining the electrolyte ion concentration. Thus, one can choose the suitable preconcentration method depending on the requirements. For example, drying method is better if the concentration of background ion does not matter. However, since there are many cases where background electrolyte should not be concentrated,[79,80] the ICP preconcentrator is also useful in those cases. Thus, while our radial layout has the clear limitation as mentioned, it is still feasible on those applications. In this sense, the bufferchannel-less radial preconcentrator and online extractor was expected for handy platform of the sample preparation step in various biomedical and environmental applications, requiring an appropriate preconcentration ratio.

SUPPLEMENTARY MATERIAL

See the supplementary material for gas production by Faradaic reaction and experimental demonstration at high buffer concentration.

ACKNOWLEDGMENTS

This work is supported by Basic Research Laboratory Project (No. NRF-2018R1A4A1022513), Basic Science Research Program (No. 2016R1A6A3A11930759), and the Center for Integrated Smart Sensor funded as Global Frontier Project (No. CISS-2011-0031870) by the Ministry of Science and ICT, Korean Health Technology RND project from the Ministry of Health and Welfare Republic of Korea (Nos. HI13C1468 and HI14C0559). Also, all authors acknowledged financial supports from BK21 plus program of Creative Research Engineer Development IT, Seoul National University. H. Y. Kim acknowledged financial support from the National Research Foundation (Grant No. 2018052541).

REFERENCES

[1]A. Arora, G. Simone, G. B. Salieb-Beugelaar, J. T. Kim, and A. Manz, Anal. Chem. **82**, 4830–4847 (2010).
[2]D. R. Reyes, D. Iossifidis, P.-A. Auroux, and A. Manz, Anal. Chem. **74**, 2623–2636 (2002).
[3]P.-A. Auroux, D. Iossifidis, D. R. Reyes, and A. Manz, Anal. Chem. **74**, 2637–2652 (2002).
[4]J. Khandurina, S. C. Jacobson, L. C. Waters, R. S. Foote, and J. M. Ramsey, Anal. Chem. **71**, 1815–1819 (1999).
[5]S. Song, A. K. Singh, and B. J. Kirby, Anal. Chem. **76**, 4589–4592 (2004).
[6]A. Zularisam, A. Ismail, and R. Salim, Desalination **194**, 211–231 (2006).
[7]D. Di Carlo, D. Irimia, R. G. Tompkins, and M. Toner, Proc. Natl. Acad. Sci. U.S.A. **104**, 18892–18897 (2007).
[8]W. Connacher, N. Zhang, A. Huang, J. Mei, S. Zhang, T. Gopesh, and J. Friend, Lab Chip **18**, 1952–1996 (2018).
[9]D. Lee, J. A. Lee, H. Lee, and S. J. Kim, Sci. Rep. **9**, 2336 (2019).
[10]J. A. Lee, D. Lee, S. Park, H. Lee, and S. J. Kim, Sci. Rep. **8**, 12842 (2018).
[11]H. Lee, J. Kim, J. Yang, S. W. Seo, and S. J. Kim, Lab Chip **18**, 1713–1724 (2018).
[12]S. Shin, J. T. Ault, P. B. Warren, and H. A. Stone, Phys. Rev. X **7**, 041038 (2017).
[13]S. Shin, E. Um, B. Sabass, J. T. Ault, M. Rahimi, P. B. Warren, and H. A. Stone, Proc. Natl. Acad. Sci. U.S.A. **113**, 257–261 (2016).
[14]J. T. Ault, P. B. Warren, S. Shin, and H. A. Stone, Soft Matter **13**, 9015–9023 (2017).
[15]D. Vigolo, R. Rusconi, H. A. Stone, and R. Piazza, Soft Matter **6**, 3489–3493 (2010).
[16]M. Yang and M. Ripoll, Soft Matter **12**, 8564–8573 (2016).
[17]B. Jung, R. Bharadwaj, and J. G. Santiago, Anal. Chem. **78**, 2319–2327 (2006).
[18]D. Bottenus, T. Z. Jubery, Y. Ouyang, W.-J. Dong, P. Dutta, and C. F. Ivory, Lab Chip **11**, 890–898 (2011).
[19]J. Lichtenberg, E. Verpoorte, and N. F. de Rooij, Electrophoresis **22**, 258–271 (2001).
[20]W. Wei, G. Xue, and E. S. Yeung, Anal. Chem. **74**, 934–940 (2002).
[21]S. D. Arnett and C. E. Lunte, Electrophoresis **24**, 1745–1752 (2003).
[22]N. P. Beard, C. X. Zhang, and A. J. demello, Electrophoresis **24**, 732–739 (2003).
[23]B. Jung, R. Bharadwaj, and J. G. Santiago, Electrophoresis **24**, 3476–3483 (2003).
[24]S. J. Kim, Y.-A. Song, and J. Han, Chem. Soc. Rev. **39**, 912–922 (2010).
[25]S. Y. Son, S. Lee, H. Lee, and S. J. Kim, BioChip J. **10**, 251–261 (2016).
[26]Y.-C. Wang, A. L. Stevens, and J. Han, Anal. Chem. **77**, 4293–4299 (2005).
[27]L. M. Fu, H. H. Hou, P. H. Chiu, and R. J. Yang, Electrophoresis **39**, 289–310 (2018).
[28]Y.-Y. Chen, P.-H. Chiu, C.-H. Weng, and R.-J. Yang, Biomicrofluidics **10**, 014119 (2016).
[29]S. Park, H. Moon, D. Lee, H. Kim, and H. Chun, Int. J. Lab. Hematol. **35**, 480–490 (2013).
[30]S. I. Han, Y. K. Yoo, J. Lee, C. Kim, K. Lee, T. H. Lee, H. Kim, D. S. Yoon, K. S. Hwang, and R. Kwak, Sens. Actuators B Chem. **268**, 485–493 (2018).
[31]W. Ouyang, X. Ye, Z. Li, and J. Han, Nanoscale **10**, 15187–15194 (2018).
[32]S. A. Hong, Y.-J. Kim, S. J. Kim, and S. Yang, Biosens. Bioelectron. **107**, 103–110 (2018).
[33]Q. Pu, J. Yun, H. Temkin, and S. Liu, Nano Lett. **4**, 1099–1103 (2004).
[34]S. J. Kim, Y.-C. Wang, J. H. Lee, H. Jang, and J. Han, Phys. Rev. Lett. **99**, 044501 (2007).
[35]S. Sohn, I. Cho, S. Kwon, H. Lee, and S. J. Kim, Langmuir **34**, 7916–7921 (2018).
[36]I. Cho, W. Kim, J. Kim, H.-Y. Kim, H. Lee, and S. J. Kim, Phys. Rev. Lett. **116**, 254501 (2016).
[37]S. Nam, I. Cho, J. Heo, G. Lim, M. Z. Bazant, D. J. Moon, G. Y. Sung, and S. J. Kim, Phys. Rev. Lett. **114**, 114501 (2015).
[38]W. Kim, S. Park, K. Kim and S. J. Kim, Lab Chip, 2017, **17**, 3841–3850.
[39]H.-C. Chang and G. Yossifon, Biomicrofluidics **3**, 012001 (2009).
[40]G. Yossifon and H.-C. Chang, Phys. Rev. Lett. **101**, 254501 (2008).
[41]S. Park, Y. Jung, S. Y. Son, I. Cho, Y. Cho, H. Lee, H.-Y. Kim, and S. J. Kim, Nat. Commun. **7**, 11223 (2016).
[42]C. L. Druzgalski, M. B. Andersen, and A. Mani, Phys. Fluids **25**, 110804 (2013).
[43]M. B. Andersen, M. van Soestbergen, A. Mani, H. Bruus, P. M. Biesheuvel, and M. Z. Bazant, Phys. Rev. Lett. **109**, 108301 (2012).
[44]I. Rubinstein and B. Zaltzman, Adv. Colloid Interface Sci. **159**, 117–129 (2010).
[45]G. Yossifon, P. Mushenheim, Y. C. Chang, and H. C. Chang, Phys. Rev. E **79**, 046305 (2009).
[46]L. F. Cheow, A. Sarkar, S. Kolitz, D. Lauffenburger, and J. Han, Anal. Chem. **86**, 7455–7462 (2014).
[47]J. Choi, K. Huh, D. J. Moon, H. Lee, S. Y. Son, K. Kim, H. C. Kim, J.-H. Chae, G. Y. Sung, H.-Y. Kim, J. W. Hong, and S. J. Kim, RSC Adv. **5**, 66178–66184 (2015).
[48]C.-H. Chen, A. Sarkar, Y.-A. Song, M. A. Miller, S. J. Kim, L. G. Griffith, D. A. Lauffenburger, and J. Han, J. Am. Chem. Soc. **133**, 10368–10371 (2011).
[49]Y.-C. Wang and J. Han, Lab Chip **8**, 392–394 (2008).
[50]S. H. Ko, S. J. Kim, L. F. Cheow, L. D. Li, K. H. Kang, and J. Han, Lab Chip **11**, 1351–1358 (2011).
[51]S. H. Ko, Y.-A. Song, S. J. Kim, M. Kim, J. Han, and K. H. Kang, Lab Chip **12**, 4472–4482 (2012).
[52]K. D. Huang and R. J. Yang, Electrophoresis **29**, 4862–4870 (2008).
[53]M. Jia and T. Kim, Anal. Chem. **86**, 10365–10372 (2014).
[54]M. Kim, M. Jia, and T. Kim, Analyst **138**, 1370–1378 (2013).
[55]S. H. Ko, S. J. Kim, and J. Han, U.S. Patent 12/958,465 (March 12, 2010).
[56]M. B. Andersen, K. M. Wang, J. Schiffbauer, and A. Mani, Electrophoresis **38**, 702–711 (2017).
[57]S. Alizadeh and A. Mani, Langmuir **33**, 6205–6219 (2017).
[58]S. M. Davidson, M. B. Andersen, and A. Mani, Phys. Rev. Lett. **112**, 128302 (2014).
[59]S. M. Rubinstein, G. Manukyan, A. Staicu, I. Rubinstein, B. Zaltzman, R. G. H. Lammertink, F. Mugele, and M. Wessling, Phys. Rev. Lett. **101**, 236101 (2008).
[60]T. Pundik, I. Rubinstein, and B. Zaltzman, Phys. Rev. E **72**, 061502 (2005).
[61]G. Yossifon, P. Mushenheim, and H. C. Chang, Europhys. Lett. **90**, 64004 (2010).
[62]G. Yossifon, P. Mushenheim, Y. C. Chang, and H. C. Chang, Phys. Rev. E **81**, 066317 (2010).
[63]E. V. Dydek, B. Zaltzman, I. Rubinstein, D. S. Deng, A. Mani, and M. Z. Bazant, Phys. Rev. Lett. **107**, 118301 (2011).
[64]J. Kim, I. Cho, H. Lee, and S. J. Kim, Sci. Rep. **7**, 5091 (2017).
[65]K. Kim, W. Kim, H. Lee, and S. J. Kim, Nanoscale **9**, 3466–3475 (2017).
[66]P. Kim, S. J. Kim, K.-Y. Suh, and J. Han, Nano Lett. **10**, 16–23 (2010).
[67]S. J. Kim, S. H. Ko, R. Kwak, J. D. Posner, K. H. Kang, and J. Han, Nanoscale **4**, 7406–7410 (2012).
[68]H. Lee, J. Choi, E. Jeong, S. Baek, H. C. Kim, J.-H. Chae, Y. Koh, S. W. Seo, J.-S. Kim, and S. J. Kim, Nano Lett. **18**, 7642–7650 (2018).
[69]B. Scarff, C. Escobedo, and D. Sinton, Lab Chip **11**, 1102–1109 (2011).

[70]J. H. Lee, Y.-A. Song, and J. Han, Lab Chip **8**, 596–601 (2008).
[71]S. E. Fosdick, K. N. Knust, K. Scida, and R. M. Crooks, Angew. Chem., Int. Ed. **52**, 10438–10456 (2013).
[72]K. N. Knust, D. Hlushkou, R. K. Anand, U. Tallarek, and R. M. Crooks, Angew. Chem. Int. Ed. **52**, 8107–8110 (2013).
[73]S. J. Kim, L. D. Li, and J. Han, Langmuir **25**, 7759–7765 (2009).
[74]A. Sze, D. Erickson, L. Ren, and D. Li, J. Colloid Interface Sci. **261**, 402–410 (2003).
[75]H. Bruus, *Theoretical Microfluidics* (Oxford University Press, Oxford, 2008).
[76]J. A. Schellman and D. Stigter, Biopolymers **16**, 1415–1434 (1977).
[77]T. A. Zangle, A. Mani, and J. G. Santiago, Chem. Soc. Rev. **39**, 1014–1035 (2010).
[78]R. Kwak and J. Han, J. Phys. Chem. Lett. **9**, 2991–2999 (2018).
[79]L. A. Haff and I. P. Smirnov, Genome Res. **7**, 378–388 (1997).
[80]P. Ross, L. Hall, I. Smirnov, and L. Haff, Nat. Biotechnol. **16**, 1347 (1998).